Proceedings of the 2006 IEEE
International Conference on Control Applications
Munich, Germany, October 4-6, 2006

Speed Control of Quadrupedal Bounding Using a Reaction Wheel

Nicholas Cherouvim and Evangelos Papadopoulos, *Senior Member, IEEE*

Abstract— **To date, quadruped speed control has either been achieved with two actuators per leg, or with single actuators and time consuming trial and error experimentation for controller tuning. In this paper, a novel control method is developed that uses only one actuator per leg and yet requires no controller tuning from the user, since the control parameters are computed through analytical expressions derived from the robot dynamics. One further actuator is used to drive a reaction wheel situated on the body. The control method leads to stable bounding gaits with controllable forward speed, and as the control is based on analytical results from the robot dynamics, it is applicable to a range of design parameters, rather than a specific robot. Light, off-the-shelf DC motors are shown to be adequate for successful controller operation. Results are shown of the control applied to a detailed robot model, including leg and toe mass, foot collision, DC motor model, joint friction and a foot-ground friction model allowing foot slipping.**

Index Terms— **speed control, quadruped robot, bounding.**

I. Introduction

Legged robots, although a relatively recent area, have become the focus of intense research, due to their huge potential for achieving efficient locomotion over varied terrain. Research has been carried out on many legged systems, from one-legged robots [1], [2], to robots with six legs or more. Both the passive [3] and the controlled dynamics [2] of such systems have been addressed to some extent, and a variety of gaits have been studied.

Quadrupeds are a class of legged robots drawing particular attention, as they are statically stable, unlike most one or two legged robots, but also retain simpler dynamics than robots with six legs or more. Quadruped robots are potentially capable of a number of gaits, the principle of which are the bound, the gallop and the trot.

In an earlier work, Raibert achieved quadruped stable locomotion using two hydraulic actuators per leg, and an external power source, [2], and was able to control forward speed. Since then, many other approaches have been made.

A significant development was the Scout II quadruped, as stable gaits were achieved with only one actuator per leg [4], [5]. The applied open loop speed control required control parameters previously determined by trial and error. Also with one actuator per leg, stable gaits were achieved using oscillatory trajectories for the legs, although speed control required experimentally investigating the effect of oscillator frequency, [6]. Finally, a case of speed setting is reported for a walking gait at slow speeds, [7].

Work also exists using two actuators per leg. With delayed feedback control, bounding is stabilized, though forward speed may not be directly set, [8]. Fuzzy control has also been employed, [9], [10]. It is used to set the speed for a galloping gait [9], while CPG's are used to control the Tekken quadruped, with three actuators per leg, [11].

Despite the progress made with quadrupeds, it is evident that a basic control problem still remains. Namely, that although robot stabilization can be achieved using one actuator per leg, forward speed setting in a running gait requires time-consuming experimental determination of controller parameters. As mentioned, speed setting may be accomplished without tuning, at the expense of using twice the number of actuators. However, the number of actuators per leg is crucial, as any increase in their number complicates design and has a quadruple effect on weight and cost, requiring more motion transmission mechanisms, and increasing power supply demands. Therefore it is essential to keep the number of actuators to a minimum.

In this work, a novel speed control method is developed that uses only one actuator per leg and one to drive a reaction wheel, and does not require experimental setting of controller parameters. It is shown how, using just one extra actuator above the minimum, stable bounding *and* setting the forward speed are achieved by designing the control through an analysis of the robot dynamics, leading to systematic computation of controller parameters. Further, this allows the controller to perform over a wide speed range and for various robot parameters. The validity of the control method is demonstrated by a realistic robot model simulated in Working Model 2D software, including real world characteristics, such as leg mass, foot collision, motor models, joint friction and foot slipping.

II. Robot Dynamics

The robot studied in this work is a quadruped with springy legs. Each leg is connected to the robot body through an actuated hip. Also, a reaction wheel is located on the robot body, to assist with attitude control during flight. The gait studied is the bound, in which the front legs are always in phase, as is the back pair. The robot goes through four motion phases in one cycle, see Fig. 1a, and is studied in the forward motion plane, using the planar model in Fig. 1b.

This work is co-funded by public funds (European Social Fund 75% and General Secretariat for Research and Technology 25%) and private funds (Zenon S.A), within measure 8.3 of Op. Pr. Comp., 3rd CSP - PENED 2003.

N. Cherouvim is with the Department of Mechanical Engineering, National Technical University of Athens, Athens, 15780, Greece. (e-mail: ndcher@mail.ntua.gr).

E. Papadopoulos is with the Department of Mechanical Engineering, National Technical University of Athens, Athens, 15780, Greece (e-mail: egpapado@central.ntua.gr, phone: +(30) 210-772-1440, fax: +(30) 210-772-1455).

The planar model, used for controller design, consists of the robot body, supported on two springy massless stick legs, actuated at the hip. Each modeled leg has twice the spring stiffness of the robot leg and includes viscous friction modeling. The reaction wheel is modeled as an actuated disk of inertia i_w. The front leg is actuated by a torque τ_f, while the back by a torque τ_b. The torque supplied by the reaction wheel is τ_w. Quantities used are shown in Table 1.

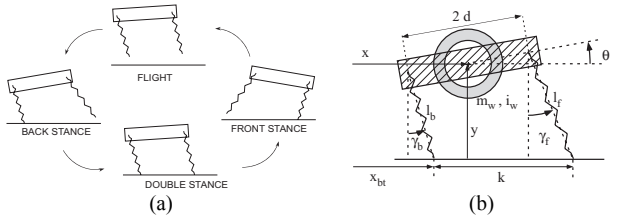

Fig. 1. The quadruped motion phases during bounding, and the robot planar model.

The robot dynamics are derived using a Lagrangian formulation and Cartesian variables x, y, θ as generalized coordinates, describing center of mass (COM) position and body attitude. Also, γ_w is the reaction wheel absolute angle. Ground impact is not studied, as the legs are massless.

TABLE 1
VARIABLES AND INDICES USED IN THE WORK

x	COM horizontal position	L	leg rest length
y	COM vertical position	g	acceleration of gravity
θ	body pitch angle	m_w	reaction wheel mass
l	leg length	i_w	reaction wheel inertia
γ	leg absolute angle	$T_{fl,1}$	apex to touchdown time
k	double stance toe distance	T_{fl}	flight duration
γ_w	reaction wheel absolute angle	$\gamma_{b,td}$	back leg touchdown angle
x_{bt}	back toe horizontal position	$\gamma_{f,td}$	front leg touchdown angle
k_b	back leg spring stiffness	w	*as index*: reaction wheel
k_f	front leg spring stiffness	f	*as index*: front leg
m	total robot mass	b	*as index*: back leg
i	body inertia	ap	*as index*: apex position
d	hip joint to COM distance	$bs0$	*as index*: back stance beginning
b	viscous friction coefficient	$ds0$	*as index*: double stance beginning

The dynamics for any phase may be derived from that of the double stance, by removing terms not pertinent to the phase. Hence only the double stance dynamics is given, as a set of differential and algebraic equations:

$$\begin{aligned} &m\ddot{x} - b\sin(\gamma_b)\dot{l}_b + \cos(\gamma_b)\tau_b/l_b + \sin(\gamma_b)k_b\left(L - l_b\right) \\ &-b\sin(\gamma_f)\dot{l}_f + \cos(\gamma_f)\tau_f/l_f + \sin(\gamma_f)k_f\left(L - l_f\right) = 0 \end{aligned} \tag{1}$$

$$\begin{aligned} &m\ddot{y} + mg - \cos(\gamma_b)k_b\left(L - l_b\right) + b\cos(\gamma_b)\dot{l}_b + \sin(\gamma_b)\tau_b/l_b \\ &-\cos(\gamma_f)k_f\left(L - l_f\right) + b\cos(\gamma_f)\dot{l}_f + \sin(\gamma_b)\tau_f/l_f = 0 \end{aligned} \tag{2}$$

$$\begin{aligned} &i\ddot{\theta} + d\cos(\gamma_b - \theta)k_b\left(L - l_b\right) - d\cos(\gamma_f - \theta)k_f\left(L - l_f\right) \\ &-bd\cos(\gamma_b - \theta)\dot{l}_b + bd\cos(\gamma_f - \theta)\dot{l}_f - \tau_w \\ &-\left(d\sin\left(\gamma_b - \theta\right) - l_b\right)\tau_b/l_b + \left(d\sin\left(\gamma_f - \theta\right) + l_f\right)\tau_f/l_f = 0 \end{aligned} \tag{3}$$

$$i_w\ddot{\gamma}_w + \tau_w = 0 \tag{4}$$

where:

$$\gamma_b = \tan^{-1}\left(y - d\sin(\theta), x_{bt} + d\cos(\theta) - x\right) \tag{5}$$

$$\gamma_f = \tan^{-1}\left(y + d\sin(\theta), k + x_{bt} - d\cos(\theta) - x\right) \tag{6}$$

$$l_b = \sqrt{\left(-x + x_{bt} + d\cos(\theta)\right)^2 + \left(y - d\sin(\theta)\right)^2} \tag{7}$$

$$l_f = \sqrt{\left(k - x + x_{bt} - d\cos(\theta)\right)^2 + \left(y + d\sin(\theta)\right)^2} \tag{8}$$

III. CONTROLLER OBJECTIVES & DESIGN METHOD

The controller objective is to ensure stable bounding, and arbitrary setting of the forward speed. During stable bounding, the leg touchdown angles and the robot state at the flight phase apex, later referred to as the motion parameters, remain unchanged over each cycle. Therefore, to achieve stable bounding with a given forward speed, the controller is designed to drive the robot to a gait matching a set of *desired* steady-state motion parameters. As a result, the initial aim is to compute the desired motion parameters of steady state bounding with the desired forward speed. This is based on an analytical analysis of the dynamics, as a numerical approach is not feasible for real-time control.

Once the motion parameters are known, the controller has three discreet functions, firstly, setting the back and front legs to their touchdown angles, secondly, maintaining the forward speed equal to the desired value, and finally controlling body pitch during flight. The forward speed $\dot{x}$ of the robot COM is maintained constant through all motion phases, using the hip actuators and a computed torque approach. This ensures good forward speed control and simplifies the analysis, as the forward speed can be regarded as constant and known. Any necessary corrections of robot attitude are done during the flight phase, using the reaction wheel. Finally, the massless model legs may be brought to their touchdown angles during flight with zero torque.

In Section IV, an analysis of the bounding gait is presented. Using this analysis, the method for motion parameter computation is laid out in Section V. Then, the final form of the controller is given in detail, in Section VI.

IV. ANALYSIS OF STEADY STATE BOUNDING

To compute the desired motion parameters, an analysis of *steady state* bounding is first made in this section, from which analytical expressions will be derived, to then lead to motion parameter computation. The desired steady state motion parameters, required for control, are the forward speed, the apex COM height, the leg touchdown angles, and the pitch and pitch velocity of the body at apex. Of the six parameters mentioned above, the forward speed and apex height are set by the user. Also, the body pitch at apex is desired to be zero. Therefore the remaining steady-state motion parameters, to be found, are the body pitch velocity at apex and the front and back leg touchdown angles.

Note, as mentioned in the previous section, that the forward speed $\dot{x}$ is kept equal to its desired value all through the cycle, and this is made use of below. Moreover, due to the complexity of the system dynamics, certain approximations are made to derive analytical expressions, which otherwise would be unobtainable. This does not invalidate the control method. If no approximations were made for computing the steady state motion parameters, then the only torque required for the motion would be to keep $\dot{x}$

constant. Given that certain approximations are made, the reaction wheel is also needed to stabilize the motion.

In all expressions in this section, time t starts at the beginning of the respective motion phase. Also, the reaction wheel torque is zero in this section, since the aim is to compute motion parameters that require no attitude correction. Below is an analysis of the steady state bounding gait, leading to the analytical expressions which allow the computation of the motion parameters in Section V.

A. Approximate solution for the back leg axial motion.

First, the evolution of the back leg length l_b is studied.

Back stance: Using simple algebra and (1)-(8), the back leg acceleration $\ddot{l}_b$, during the back stance phase, is written as a function of l_b, γ_b, θ, in which the terms containing the torque τ_b are neglected, when compared to the magnitude of the spring force terms. So, $\ddot{l}_b$ is found as:

$$\begin{aligned}\ddot{l}_b = \frac{1}{2im}\Big[& k_b\left(L-l_b\right)\left(2i+md^2+md^2\cos\left(2\left(\gamma_b-\theta\right)\right)\right) \\ & -b\dot{l}_b-2gim\cos\left(\gamma_b\right)+2im\left(l_b\dot{\gamma}_b^2-d\sin\left(2\left(\gamma_b-\theta\right)\right)\dot{\theta}^2\right)\Big]\end{aligned} \quad (9)$$

As values of θ, γ_b are generally small, (9) becomes:

$$im\ddot{l}_b = k_b(L-l_b)(i+md^2)-gim-b\dot{l}_b+iml_b\dot{\gamma}_b^2 \quad (10)$$

Further, if terms representing viscous friction and centrifugal force are considered small enough in comparison to the spring forces, then the back leg length dynamics is:

$$im\ddot{l}_b = k_b(L-l_b)(i+md^2)-gim \quad (11)$$

Equation (11) is a second-order oscillator, whose solution is:

$$l_b = g\cos(\omega_1\cdot t)/\omega_1^2+\dot{l}_{b,bs0}\sin(\omega_1\cdot t)/\omega_1+L-g/\omega_1^2 \quad (12)$$

where $\omega_1 = (k_b(i+md^2)/im)^{1/2}$,

and $\dot{l}_{b,bs0}$ is the back leg axial velocity at the beginning of the back stance phase.

Double stance: For the double stance phase, using similar simplifications as previously, the back leg length equation is:

$$m\ddot{l}_b = 2k_b(L-l_b)-gm \quad (13)$$

Again, the solution is:

$$l_b = \left(l_{b,ds0}-L+\frac{g}{\omega_2^2}\right)\cos\left(\omega_2\cdot t\right)+\frac{\dot{l}_{b,ds0}}{\omega_2}\sin\left(\omega_2\cdot t\right)+L-\frac{g}{\omega_2^2} \quad (14)$$

where $\omega_2 = \sqrt{2k_b/m}$,

and $\dot{l}_{b,ds0}$ is the back leg axial velocity at the beginning of double stance. It is evident that the back leg axial dynamics differ from back stance to double stance. Note that the two are the same only in the case where $i = md^2$.

Unified approximation for $l_b(t)$ during both phases: The back leg length equation has an oscillatory form during both the back and the double stance phase, differing only in the natural frequencies ω_1 and ω_2, as can be seen in (12), (14). An oscillation of the same form is now used as an approximate *single* unified expression for $l_b(t)$ across both the back *and* the double stance phase. In this oscillation, the natural frequency ω is equal to neither ω_1 or ω_2, and needs determining. The unified $l_b(t)$ expression is:

$$l_b = g\cos(\omega\cdot t)/\omega^2+\dot{l}_{b,bs0}\sin(\omega\cdot t)/\omega+L-g/\omega^2 \quad (15)$$

To obtain the correct value for the natural frequency ω, the back leg length is recorded at the point of its maximum compression during the previous cycle, using the robot sensors. From (15), the back leg length l_{bot} at its maximum compression can be expressed analytically:

$$l_{bot} = L-g/\omega^2-\sqrt{\left(g/\omega^2\right)^2+\dot{l}_{b,bs0}^2/\omega^2} \quad (16)$$

Equating l_{bot} from (16) with the recorded value $l_{bot,r}$, the natural frequency ω can be computed as:

$$\omega = \sqrt{(2gL+\dot{l}_{b,bs0,i-1}^2-2gl_{bot,r})}/(L-l_{bot,r}) \quad (17)$$

where $\dot{l}_{b,bs0,i-1}$ is $\dot{l}_{b,bs0}$ measured at the previous cycle. Computing ω from the real data of the previous cycle is significant, as it gives a more reliable prediction for the leg length, despite approximations made.

B. Body pitching during back stance.

During the back stance phase, the body pitch dynamics is given by (3), by removing terms not pertinent to the phase:

$$\begin{aligned}i\ddot{\theta} = & -d\cos(\gamma_b-\theta)k_b(L-l_b)+bd\cos(\gamma_b-\theta)\dot{l}_b \\ & +\tau_w+(d\sin(\gamma_b-\theta)/l_b-1)\tau_b\end{aligned} \quad (18)$$

As previously, the reaction wheel torque is assumed to be zero. Using the same small angle assumptions as above, and again neglecting the terms corresponding to viscous friction and the torque τ_b, as explained above, (18) becomes:

$$i\ddot{\theta} = -dk_b(L-l_b) \quad (19)$$

Using (15) in (19), it can be found that:

$$\theta = \left(dk_b/i\omega^2\right)\left(-l_b+L-g/\omega^2-gt^2/2+c_1t+c_0\right) \quad (20)$$

where $c_1 = i\omega^2\dot{\theta}_{bs0}/\left(dk_b\right)+\dot{l}_{b,bs0}$, $c_0 = i\omega^2\theta_{bs0}/\left(dk_b\right)+g/\omega^2$.

Also, θ_{bs0} is the body pitch, and $\dot{\theta}_{bs0}$ the pitch velocity at the beginning of back stance. As the duration of the back stance is short, the term quadratic in t in (20) is small. Then, applying (20) at the end of the back stance yields:

$$\dot{\theta}_{ds0} = \dot{\theta}_{bs0}+dk_b(\dot{l}_{b,bs0}-\dot{l}_{b,ds0})/(i\omega^2) \quad (21)$$

where $\dot{\theta}_{ds0}$, $\dot{l}_{b,ds0}$ are the pitch velocity and back leg axial velocity at the beginning of double stance. As will be seen in Section VI, to reduce the effects of the approximations made in (20), the controller forces the pitch during the back stance phase along the trajectory described in (20).

C. Flight phase.

During the steady state motion, the robot COM reaches an apex height h, at which $\theta = 0$. During flight, $\dot{\theta} = \dot{\theta}_{bs0} = const.$ since the reaction wheel torque is zero and the legs are massless. The condition for the touchdown of the back leg, marking the beginning of back stance, is:

$$y = L\cos(\gamma_{b,td})+d\sin(\theta_{bs0}) \quad (22)$$

If $T_{fl,1}$ is the duration of the flight phase from apex to the beginning of back stance, then the pitch angle θ_{bs0} is:

$$\theta_{bs0} = \dot{\theta}_{ap}T_{fl,1} \quad (23)$$

Using (23), and for small θ, (22) becomes:

$$y = L\cos(\gamma_{b,td})+d\dot{\theta}_{bs0}T_{fl,1} \quad (24)$$

During flight, the body COM vertical motion equation is:

$$y = h - gt^2/2 \tag{25}$$

Combining (24), (25) at touchdown, $T_{fl,1}$ is found:

$$T_{fl,1} = \left(-d\dot{\theta}_{bs0} + \sqrt{2gh + d^2\dot{\theta}_{bs0}^2 - 2gL\cos(\gamma_{b,td})}\right)/g \tag{26}$$

The vertical velocity $\dot{y}$ at the beginning of back stance, $\dot{y}_{bs0}$, can now be found:

$$\dot{y}_{bs0} = -gT_{fl,1} \tag{27}$$

From the velocity transformations at touchdown, the back leg axial velocity at the beginning of back stance is:

$$\dot{l}_{b,bs0} = \dot{y}_{bs0}\cos(\gamma_{b,td}) - \dot{x}\sin(\gamma_{b,td}) - d\cos(\gamma_{b,td} - \theta_{bs0})\dot{\theta}_{bs0} \tag{28}$$

D. Mode of bounding.

The back leg length l_b is given by (15), so the back leg length at its maximum compression is:

$$l_{bot} = L - g/\omega^2 - \sqrt{(g/\omega^2)^2 + \dot{l}_{b,bs0}^2/\omega^2} \tag{29}$$

From (15), the time the back leg is on the ground, T_{st}, is:

$$T_{st} = 2\left(\arctan((\dot{l}_{b,bs0}\cdot\omega)/g) + \pi\right)/\omega \tag{30}$$

To ensure a bounding gait of good form, with non-trivial phases, it is desired that the duration of the back stance phase during the steady state motion will be equal to half the time the back leg is in contact with the ground. Therefore,

$$T_{bs} = T_{st}/2 \tag{31}$$

In this case, using (15), it is readily found that at the beginning of the double stance phase, the following hold:

$$\dot{l}_{b,ds0} = 0,\ l_{b,ds0} = l_{bot} \tag{32}$$

E. Absolute leg angles γ_b, γ_f.

At some point while the back leg is on the ground, and since $\dot{x}$ is constant, it can be seen from Fig. 1, that:

$$L\sin(\gamma_{b,td}) - l_b\sin(\gamma_b) = \dot{x}t + d\left(\cos(\theta_{bs0}) - \cos(\theta)\right) \tag{33}$$

Therefore, for small γ_b, θ it follows that:

$$\gamma_b = (-\dot{x}t + L\gamma_{b,td})/l_b \tag{34}$$

and

$$\dot{\gamma}_b = (-\dot{x}l_b - \dot{l}_b(-\dot{x}t + L\gamma_{b,td}))/l_b^2 \tag{35}$$

Similarly, for the front leg, it is:

$$\gamma_f = (-\dot{x}t + L\gamma_{f,td})/l_f \tag{36}$$

$$\dot{\gamma}_f = (-\dot{x}l_f - \dot{l}_f(-\dot{x}t + L\gamma_{f,td}))/l_f^2 \tag{37}$$

Note that for (34), (35) time t begins with the back stance phase, and for (36), (37) with the double stance phase.

F. Double stance.

During the double stance phase and for small θ, the following expression can be derived from Fig. 1:

$$2d\theta = l_f\cos(\gamma_f) - l_b\cos(\gamma_b) \tag{38}$$

Taking the derivative:

$$\begin{aligned} 2d\dot{\theta} = {} & \dot{l}_f\cos(\gamma_f) - l_f\dot{\gamma}_f\sin(\gamma_f) \\ & -\dot{l}_b\cos(\gamma_b) + l_b\dot{\gamma}_b\sin(\gamma_b) \end{aligned} \tag{39}$$

At the double stance beginning, solving (39) for $\dot{l}_{f,ds0}$ gives:

$$\begin{aligned} \dot{l}_{f,ds0} = {} & \left(l_{f,ds0}\dot{\gamma}_{f,ds0}\sin(\gamma_{f,td}) + \dot{l}_{b,ds0}\cos(\gamma_{b,ds0})\right. \\ & \left. -l_{b,ds0}\dot{\gamma}_{b,ds0}\sin(\gamma_{b,ds0}) + 2d\dot{\theta}_{ds0}\right)/\cos(\gamma_{f,td}) \end{aligned} \tag{40}$$

where $\gamma_{b,ds0}$, $\dot{\gamma}_{b,ds0}$, $\dot{\gamma}_{f,ds0}$ are given by (34) to (37) and $\dot{\theta}_{ds0}$ is given by (21).

V. Computation of Motion Parameters for Steady State Motion

The above results now allow the computation of the three motion parameters set out in Section IV, namely the leg touchdown angles $\gamma_{b,td}$, $\gamma_{f,td}$ and the apex pitch velocity, for which $\dot{\theta}_{ap} = \dot{\theta}_{bs0}$ for unactuated flight. For a unique parameter solution, the three constraints below are written:

$$f_1 = \dot{l}_{b,bs0} - \dot{l}_{f,ds0} = 0 \tag{41}$$

$$f_2 = 2\theta_{bs0} - T_{fl}\dot{\theta}_{bs0} = 0 \tag{42}$$

$$f_3 = \gamma_{f,td} - \dot{x}T_{st}/(2L) = 0 \tag{43}$$

where T_{fl} is the flight duration. The constraints are chosen so as to result in a periodic motion. (a) The first constraint, (41), requires that the two leg touchdown velocities are equal. If this holds, and the evolutions of the leg lengths $l_b(t)$, $l_f(t)$, are described by expressions of the form of (15), then they will be approximately identical. Further, consider the pitch dynamics written for the double stance phase, using the assumptions prior to (19):

$$i\ddot{\theta} = -dk_b(L - l_b) + dk_f(L - l_f) \tag{44}$$

For robots with equal leg stiffness, as in this case, it appears that identical leg length evolutions provide antisymmetric pitch acceleration over the stance phases. This causes the apex pitch velocity to be the same between two apexes.

(b) The second constraint, (42), ensures that during flight the body passively acquires a pitch at touchdown, equal to minus the pitch at liftoff. This also happens in the passive case, and corrects the attitude for the next stance, [3]. (c) Finally, as the first two constraints may be achieved for many leg touchdown angles, the third constraint, (43), binds the front touchdown angle, using Raibert's analysis, [2], so that a reasonable set of touchdown angles is found.

Since an algebraic solution to the parameters is not feasible, using the constraints and the analysis of Section IV, the parameters are found iteratively using a Newton-Raphson algorithm, the flow of which is laid out in Fig. 2.

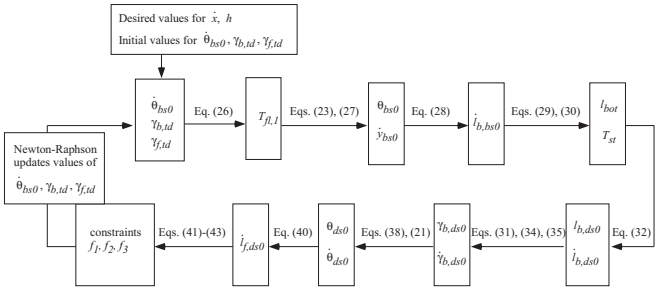

Fig. 2. The Newton-Raphson algorithm for the computation of the steady state parameters.

The algorithm convergence time on a P4 3.2 GHz Linux box is typically about 5 ms, so even on-board computation delays will be acceptable, given that the algorithm needs to

be run only once per cycle at the beginning of the flight phase, and typical flight durations are twenty to forty times longer. Convergence was the rule for reasonable bounding gaits, as will be demonstrated in Section VII for a wide range of motions. On completion of the algorithm, the parameters $\dot{\theta}_{bs0}$, $\gamma_{b,td}$, $\gamma_{f,td}$ are known, and the parameters θ_{bs0}, $\dot{l}_{b,bs0}$ are computed, as shown in Fig. 2.

VI. Controller Structure

Now that the parameters of the steady state desired motion are known, the three controller components can be laid out. Each time the desired speed or apex height is changed, the steady state motion parameters are recomputed.

A. Body pitch control.

Due to analysis approximations, the desired touchdown body attitude will not be achieved passively in reality. For this reason, the body is forced during flight to follow a pitch trajectory $\theta_d(t)$, using the reaction wheel torque τ_w. This ensures that the pitch θ_{bs0} and pitch velocity $\dot{\theta}_{bs0}$, from Section V, are obtained at touchdown. The trajectory is:

$$\theta_d = p_0 + p_1 t + p_2 t^2 + p_3 t^3 \tag{45}$$

where

$$\begin{aligned} p_0 &= \theta_{fp0}, \qquad p_2 = (\dot{\theta}_{bs0} - \dot{\theta}_{fp0} - 3 \cdot T_{traj}^2 p_3) / (2 \cdot T_{traj}) \\ p_1 &= \dot{\theta}_{fp0}, \; p_3 = (-2\theta_{bs0} + \dot{\theta}_{bs0} \cdot T_{traj} + \dot{\theta}_{fp0} \cdot T_{traj} + 2\theta_{fp0}) / T_{traj}^3 \end{aligned} \tag{46}$$

and *fp0* denotes the beginning of the flight phase, and T_{traj} is the trajectory duration, set equal to the duration of the flight phase, T_{fl}. The reaction wheel torque is:

$$\tau_w = i\ddot{\theta}_d + k_d(\dot{\theta}_d - \dot{\theta}) + k_p(\theta_d - \theta) \tag{47}$$

During the back stance phase, the reaction wheel is used to force the body pitch along the trajectory in (20), so τ_w again has the form of (47). This helps decrease the effect of the approximations made in Section IV. Finally, during the double and front stance phases, the reaction wheel motor is used to brake the wheel, so its momentum stays bounded.

B. Leg Touchdown angles.

Front leg: The front leg touchdown angle, $\gamma_{f,td}$, computed in Section V, is used at every cycle touchdown.

Back leg: Due to the approximations of Section IV, if the back leg touchdown angle computed is used, then the resulting back leg axial velocity $\dot{l}_{b,bs0}$ at touchdown will not be equal to that calculated in the analysis. However, achieving the computed value for $\dot{l}_{b,bs0}$ is particularly important, as it greatly affects the apex height, and the pitching motion, as can be seen from (20). Therefore, the back leg touchdown angle $\gamma_{b,td}$ is recomputed during each flight phase, so as to achieve the computed $\dot{l}_{b,bs0}$. If $\gamma_{b,td}$, θ_{bs0} are small, $\gamma_{b,td}$ can be recomputed from (28), while the required $\dot{y}$ is given by (27). This recomputation of the back leg angle "pulls" the system towards the desired gait.

C. Forward motion.

As mentioned, the forward COM speed $\dot{x}$ is kept equal to the desired value, using the computed torque control approach. With reference to (1), the torque is:

$$\tau_i = k_{p,1}(\dot{x} - \dot{x}_{des}) + l_i \tan(\gamma_i)(-k_i(L - l_i) + b \cdot \dot{l}_i) \tag{48}$$

where $i = b, f$.

VII. Results

In this section, simulations of a realistic robot response to the controller in Section VI are shown. In [12] it is made apparent that by including enough real-world characteristics in the robot model, the simulated behavior may match the real response to a remarkable degree. The results shown are from the simulation package Working Model 2D. The robot model includes detailed motor models with saturation, motor current amplifier limits, leg and toe mass, foot collision, friction in the leg springs and hip joints and friction between the feet and the ground. The motor and gearhead data comes from the manufacturer [13], and only widely available motors are used. As the robot legs have mass, a simple PD controller is used to bring them to their touchdown angles during flight. The gains used in (47), (48) are not critical and any reasonable value may be used, such as k_d=50, k_p=100, k_{p1}=50. Finally, although the robot user may request step changes of arbitrary size in desired speed, the controller limits changes to 0.02 m/s per cycle, to enhance stability.

The robot used has m=16 kg, $k_b = k_f$ = 7000 N/m, d= 0.24 m, i =0.8 kg·m^2, while the, fully realizable, reaction wheel has m_w=6 kg, i_w=0.15 kg·m^2. The inertia of the wheel must be selected large enough to avoid spinning at speeds beyond its motor range. The parameters for the 90 W DC motor model used at the hips are the nominal voltage $V_{\max}$ =42 V, terminal resistance r =2.07 Ω, torque constant k_T =0.05 mNm/A, while the gearhead used has a reduction of g_e =81. The reaction wheel motor is 150 W DC, and the above model parameters are $V_{\max}$ =48 V, r =1.16 Ω, k_T =0.06 mNm/A, and g_e =43. All motors weigh under 0.5 kg each, and for each motor and gearhead, the max torque permitted by the manufacturer has also been modeled. Each leg has a mass of 0.3 kg, while each foot mass has a value of 0.05 kg. The collisions of the unsprung foot masses with the ground are modeled as plastic collisions. The viscous friction coefficient is $b = 15$ N·s/m in the leg, while at the hip joint it is 0.5 N·m·s/rad. The foot-ground friction is modeled using a simple Coulomb model, with a static coefficient of 0.7, and a kinetic coefficient of 0.6. Using this model, foot slippage is observed particularly at touchdown, as the foot needs to decelerate before stopping.

In Fig. 3, simulation data is shown from the robot following a desired forward speed profile. In Fig. 4 snapshots of the same simulation are shown. The initial states of the simulation are y=0.4 m, $\dot{x}$ =1.5 m/s, $\dot{\theta}$=0 rad/s, θ=0 rad, and are not special. The desired apex height is set to h=0.41 m. Note that the *only* user inputs to the controller, for the complete motion, are the desired speed and height.

As can be seen in Fig. 3a, the robot rapidly responds to the step changes in desired velocity, although these may be large and abrupt. During a single cycle the speed is not exactly constant, due to motor saturation, and the many real-world characteristics included in the simulation. Further, although the forward speed may be set in a large range, it may not be arbitrarily small, as then it becomes impossible for adequate energy to be transferred from the hip actuators into the vertical direction of motion, so as to achieve a sustainable hopping height. In Fig. 3b the body height at apex is shown to deviate from the desired value of 0.41 m,

so the desired apex height may be seen as more of a qualitative parameter, to be studied in future work.

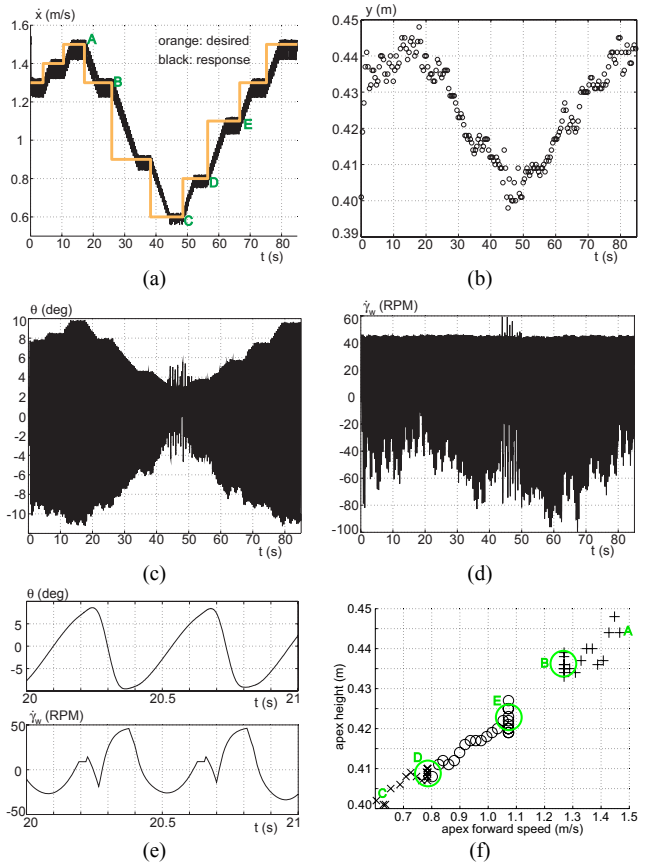

Fig. 3. Robot response to a speed trajectory. (a) Forward speed. (b) Apex body height y. (c) Body pitch θ. (d) Reaction wheel speed. (e) Detail of body pitch and wheel speed. (f) Poincare type section.

The pitch angle θ, depicted in Fig. 3c, shows that the body movement is well behaved, with no extreme configurations. The revolution speed of the reaction wheel, shown in Fig. 3d, is bounded, which is necessary to keep the wheel motor within its operating range. Despite the bounds on both θ and $\dot{\gamma}_w$, these are not analytically guaranteed, and do rely on appropriate selection of the wheel inertia. Due to the large motion time (85 s), Figs. 3c, 3d are shown only to demonstrate the bounds of their corresponding quantities. Details of the body pitch and wheel speed evolutions are given in Fig. 3e.

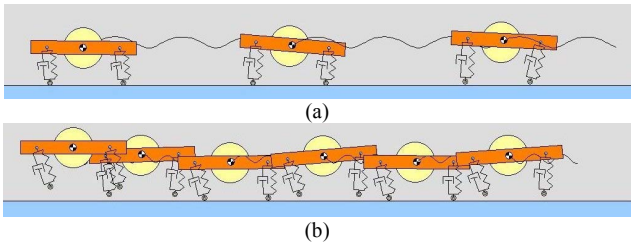

Fig. 4. Quadruped response, in Working Model 2D, with snapshots taken every 1s, (a) from time 12 s and, (b) from time 45 s, onwards.

In Fig. 3f, a Poincare type section of the motion is shown, using two robot states at each flight apex. The lettered points A, B, etc. correspond to the points shown in Fig. 3a. The Poincare section shows the motion between points A and B, C and D, D and E. The transient state between desired speeds (points wide apart) and the steady state at a desired speed (clustered points) can be seen. The clustering of points in Fig. 3e, for a constant desired speed, indicates that the robot motion could continue indefinitely at any of these speeds. This has been confirmed through simulation, but is not presented due to space restrictions.

VIII. Conclusions

In this paper, a control method was developed for the forward speed control of a bounding quadruped. Its novelty lies in that, although only one actuator per leg is used, no controller tuning or user input is required, other than the desired speed and apex height, unlike previous work in which two actuators per leg have been used, or else experimental derivation of controller parameters has been necessary. A reaction wheel is used on the body, and the control parameters are computed through analytical expressions derived from the robot dynamics. Simulations of a complete robot model showed the controller to be both fast and accurate, despite the effects of many real world characteristics. An open issue is controller generalization to the 3D case, and robot implementation is also planned.

References

[1] W. J. Schwind and D. E. Koditschek, "Control of forward velocity for a simplified planar hopping robot," *Proc. 1995 IEEE Int. Conference on Robotics & Automation,* Nagoya, Aichi, Japan, pp.691-696, 1995.

[2] M. H. Raibert, "Legged robots that balance," *MIT Press*, Cambridge, MA, 1986.

[3] I. Poulakakis, E. Papadopoulos and M. Buehler, "On the stable passive dynamics of quadrupedal running," *Proc. 2003 IEEE Int. Conference on Robotics & Automation*, Taipei, Taiwan, pp.1368-1373, Sept. 2003.

[4] S. Talebi, I. Poulakakis, E. Papadopoulos and M. Buehler, "Quadruped robot running with a bounding gait," *Proc. 7th Int. Symp. on Experimental Robotic (ISER'00)*, Honolulu, HI, pp.281-289, December 2000.

[5] D. Papadopoulos and M. Buehler, "Stable running in a quadruped robot with compliant legs," *Proc. 2000 IEEE Int. Conf. Robotics and Automation*, San Francisco, CA, pp. 444-449, April 2000.

[6] F. Iida and R. Pfeifer, "Cheap rapid locomotion of a quadruped robot: self-stabilization of bounding gait," *Proc. Intelligent Autonomous Systems 8*, IOS Press, pp. 642-649, 2004.

[7] M. Lasa and M. Buehler, "Dynamic compliant quadruped walking," *Proc. 2001 IEEE Int. Conf. on Robotics and Automation*, pp. 3153-3158, 2001.

[8] Z. Zhang, Y. Fukuoka and H. Kimura, "Adaptive running of a quadruped robot using delayed feedback control," *Proc. 2005 IEEE Int. Conf. on Robotics and Automation*, pp. 3750-3755, 2005.

[9] W. Marhefka, D. E. Orin, J. P. Schmiedeler and K. J. Waldron, "Intelligent control of quadruped gallops," *IEEE/ASME Transactions On Mechatronics*, Vol. 8, No. 4, pp. 446-456, 2003.

[10] J. G. Nichol, S. P. N. Singh, K. J. Waldron, L. R. Palmer III, D. E. Orin, "System design of a quadrupedal galloping machine", *The Int. Journal of Robotics Research*, Vol. 23, No. 10–11, pp. 1013-1027, 2004.

[11] Y. Fukuoka, H. Kimura and A. H. Cohen, "Adaptive dynamic walking of a quadruped robot on irregular terrain based on biological concepts," *The Int. Journal of Robotics Research*, Vol. 22, No. 3-4, pp. 187-202, 2003.

[12] I. Poulakakis, J. A. Smith and M. Buehler, "Modeling and experiments of untethered quadrupedal running with a bounding gait: the scout II robot," *The Int. Journal of Robotics Research*, Vol. 24, No. 4, pp. 239-256, 2005.

[13] Maxon Motor AG, www.maxonmotor.com.